6-2013

Flow-Tube Oxidation Experiments on the Carbon Preform of PICA

Francesco Panerai
University of Kentucky, francesco.panerai@uky.edu

Alexandre Martin
University of Kentucky, alexandre.martin@uky.edu

Nagi N. Mansour
NASA Ames Research Center

Steven A. Sepka
ERC, Incorporated

Jean Lachaud
University of California - Santa Cruz

Digital Object Identifier (DOI)
http://dx.doi.org/10.2514/6.2013-2769

Fluid Dynamics and Co-located Conferences
June 24-27, 2013, San Diego, CA
44th AIAA Thermophysics Conference

Flow-tube Oxidation Experiments on the Carbon Preform of PICA

Francesco Panerai* and Alexandre Martin†
University of Kentucky, Lexington, KY, USA 40506-0503

Nagi N. Mansour‡
NASA Ames Research Center, Moffett Field, CA, USA 94035

Steven A. Sepka§
ERC, Incorporated, Huntsville, AL, USA 35805

and Jean Lachaud¶
University of California Santa Cruz, Moffett Field, CA, USA 94035

Oxidation experiments on the carbon preform of a phenolic-impregnated carbon ablator were performed in the NASA Ames flow-tube reactor facility, at temperatures between 700 and 1300 K, under dry air gas at pressures between 10^3 and 10^4 Pa. Mass loss, volumetric recession and density changes were measured at different test conditions. An analysis of the diffusion/reaction competition within the porous material, based on the Thiele number, allowed us to identify low temperature and low pressure conditions to be dominated by in-depth volume oxidation. Experiments above 1000 K were found at transition conditions, where diffusion and reaction occur at similar scales. The microscopic oxidation behavior of the fibers was characterized by scanning electron microscopy and energy dispersive x-ray analysis. The material was found to oxidize at specific sites forming a pitting pattern distributed over the fibers' surface. Calcium- and oxygen-rich residues from the oxidation reactions were observed at several locations.

I. Introduction

The entry of a spacecraft into a planetary atmosphere presents a challenging high enthalpy thermo-chemical environment, requiring a suitable heat shield to protect the spacecraft and its payload from the surrounding gas. For moderate speed entry, typically below 7.5 km/s, and mild heat fluxes, up to 1 MW/m^2, reusable materials are a suitable solution. A famed example are the ceramic tiles mounted on the Space Shuttle orbiter. Entry speeds higher than 8 km/s, heat fluxes exceeding 1.5 MW/m^2, and entry into high density atmospheres impose the use of ablative thermal protection systems. These handle the incoming heating by phase changes, chemical reactions and material removal. The last decade has seen a renewed effort by scientists and engineers towards the development of a new class of low density carbon/resin ablators, made of a carbon fiber preform impregnated in phenolic resin. A successful example is the phenolic-impregnated carbon ablator (PICA) developed at NASA Ames Research Center and flight qualified during recent reentry missions, as Stardust (Earth entry at 12 km/s) and Mars Science Laboratory (Mars entry at 5.5 km/s). SpaceX has also successfully flown this class of ablators as heatshield for a commercial return capsule.

*Postdoctoral Scholar, Department of Mechanical Engineering, 261 Ralph G. Anderson Building. Visiting Scientist, Thermal Protection Materials Branch, Mail Stop 234-1, NASA Ames Research Center, Moffett Field, CA, 94035, AIAA Senior Member.
†Assistant Professor, Department of Mechanical Engineering, 261 Ralph G. Anderson Building, AIAA Senior Member.
‡Chief Scientist for Modeling and Simulation, Space Technology Division, Mail Stop 229-3, AIAA Associate Fellow.
§Senior Research Scientist, Thermal Protection Materials and Systems Branch, NASA Ames Research Center, Moffett Field, CA, 94035, AIAA Member.
¶Scientist, Silicon Valley Initiatives, NASA Ames Research Park, Building 19, AIAA Senior Member.

One of the remarkable interests of carbon/phenolic ablators is to allow the use of different carbon preforms and to adapt the properties of the impregnating matrix to the characteristics of the flight trajectory. Despite a high technology readiness level, large design margins are applied during TPS sizing due to the numerous assumptions needed on material properties and their physical response, at the expense of mass budget and cost. To help quantify design uncertainties, state of the art pyrolysis-ablation models,[1,2,3] proven as reliable engineering tools by recent missions, yet nonexempt of discrepancies with flight data,[4,5] are being revisited. A multi-scale approach has been proposed by Lachaud *et al.*[6] in order to improve understanding of the behavior of carbon/phenolic composites. One of the new features compared to state-of-the-art tools, is the development of a microscopic scale volume-averaging model for the oxidation of carbon fibers and charred phenolic-polymer matrix. Despite numerous wind tunnel tests and flight data available in the literature, dedicated testing and quantification of the different parameters and material properties is needed to validate this model. The scientific approach followed, is to implement different fundamental experiments able to decouple and separately address the various effects occurring during the ablation process of a carbon/phenolic composite.

A first validation effort, performed in a tubular reactor, addressed the oxidation of carbon preform in air at ∼900 K.[9] It proved the capability of the model to predict surface recession and oxidation penetration. It was decided to continue the study and extend the temperature and pressure ranges of this experiment.

In this paper we document oxidation experiments on the carbon preform of PICA in the NASA Ames flow-tube reactor. The material is tested under dry air at pressures from 1.6 to 60 kPa and temperatures from 700 to 1300 K, promoting the recession of the carbon fibers by oxidation reactions. As shown in Fig. 1, the leading chemical process is the oxidation of solid C into CO_2 ($C_{(s)} + O_2 \longrightarrow CO_2$) for T below 973 K (Boudouard's equilibrium) and into of CO at higher temperatures ($C_{(s)} + \frac{1}{2} O_2 \longrightarrow CO$), where the Gibbs free energy favors carbon monoxide production. It is also important to note that above the Boudouard's equilibrium, carbon removal could also occur through a separate mechanism involving carbon dioxide as reactant: $C_{(s)} + CO_2 \longrightarrow 2\,CO$.

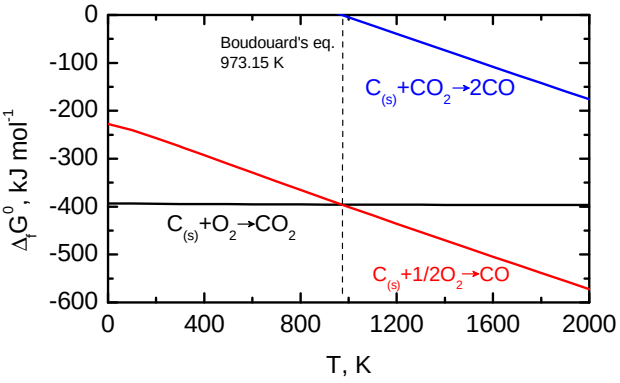

Figure 1. Ellingham diagram[7] for carbon oxidation. Gibbs free energy data are taken from NIST-JANAF tables.[8] Below the Boudouard equilibrium at 973 K the leading reaction is the oxidation C into CO_2, above 973 K Gibbs free energy favors the production of CO.

We characterized mass loss and recession of hollow cylindrical (short pipe) specimens using macroscopic and microscopic techniques. The paper intends to document a complete set of experiments and their analysis using state-of-the-art techniques.

II. Experiment

Experiments were performed in the NASA Ames flow-tube reactor shown in Fig. 2. The facility consists of a quartz main tube, connected to a right angle 2.5 cm diameter side arm, where the test section is located. High purity air (Ultra Zero Grade 99.999%, Matheson Tri-Gas®, San Jose, CA, United States) and helium (Ultra High Purity Grade 99.999%, Matheson Tri-Gas®, San Jose, CA, United States) are supplied into the reactor, upstream of the tubes intersection, and regulated using metering valves and calibrated mass flow meters (FM-360, Tylan Corp., Torrance, CA, United States). To operate the facility as a flow-tube the main arm was sealed downstream the intersection by a Teflon® valve, kept closed throughout the test. The system is evacuated using a mechanical pump, connected right before the dead-end of the side-arm. The pressure is monitored using two capacitance manometer gauges (622B Baratron®, MKS Instruments, Andover, MA, United States), operating in 1 torr and 1000 torr ranges respectively, and regulated by a PID controller of the outlet section throttle valve. The central part of the quartz side-arm is enclosed in a clam-shell electric furnace, spanning a region of approximately 470 mm, and providing temperatures up to 1500 K. Prior to testing, the specimen was placed at the middle section of the furnace using glass holders and extension tubes.

The material studied in this paper is FiberForm®, an industrial carbon preform manufactured by Fiber

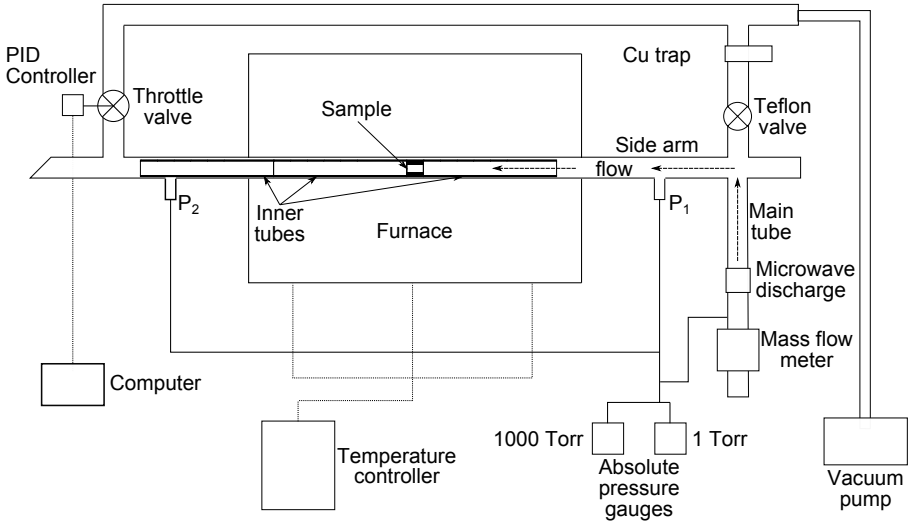

Figure 2. Schematic of the NASA Ames flow-tube test setup.

Material Inc. (Biddeford, ME, United States). It is developed for industrial thermal furnaces insulation and is selected by NASA as precursor for PICA. Sample geometry for the experiments reported, shown in Fig. 3, was a 25.4 mm height hollow cylinder, with 16 mm internal diameter and 22 mm external diameter. The specimen was interference-fit into a glass holder placed at the middle section of the heating furnace. Three 220 mm long glass tubes were placed, with contact, two upstream of the sample holder and one downstream, in order to avoid facing steps and ensure a fully developed pipe flow.

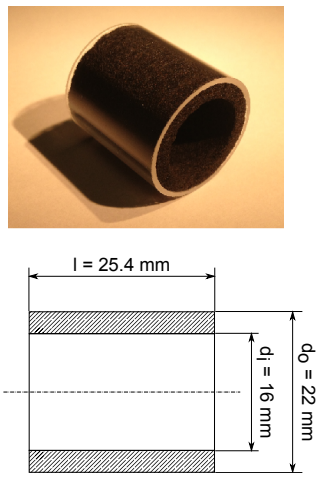

Figure 3. Hollow cylinder carbon preform sample. The top picture shows the specimen fit into the glass holder, on the bottom sketch of the specimen geometry is detailed.

The test procedure consisted in sealing the tubes, evacuating the system to a base pressure below 10 Pa and feeding it with a low helium flow (below 0.03 mg s^{-1}) while the furnace was heating up to the target temperature condition. The supply of He ensured that no oxidation reaction occurred during the transient heating phase. Once the temperature was stabilized, the He flow was stopped, the chamber was evacuated again down to 100 Pa, and dry air flow was started at the desired rate. The test gas supply caused the pressure to rise to the target value, where the regulation was taken over by the PID controller, by adjusting the suction rate of the mechanical pump downstream the samples. The transient phase to the target pressure was monitored to have a duration of ∼1 min for the lowest pressure condition (1.6 kPa) and ∼5 min for the highest value (60 kPa). Mass flow and pressure were maintained constant throughout the test time. The experiment ended with a final evacuation of the test section below 100 Pa and a restoring of the He flow, during the cooling phase of the system.

The test conditions are detailed in Table 1. We performed experiments at temperatures from 700 to 1300 K, steps of 100 K, and pressures of 1.6, 10 and 60 kPa, maintained for a total of 1 h oxidation time during each run. Gas properties were calculated using the Chemical Equilibrium with Applications (CEA) code[10] from NASA Glenn Research Center. Reynolds number $\mathrm{Re} = \rho u D/\mu$, based on the 22 mm tube diameter, was below 3.7 at all test conditions, indicating a fully laminar pipe flow.

The three pressure levels were selected to cover three different transport conditions within the porous material, as shown in Figure 4. The plot, proposed in Ref. 6, presents Knudsen number (mean free path $\bar{\lambda}$ to mean pore diameter d_p ratio) regimes from continuum to rarefied, calculated for a mean pore diameter of 50 µm for carbon preform. Experiments at 1.6, 10 and 60 kPa cover respectively continuum, slip and transition regimes within the pores of the material. The Stardust trajectory is shown as reference on the same graph

to highlight that the flow regime at the fiber scale is different than the regime at the capsule scale (typically continuum during the portion of reentry where ablation is relevant[11]). The characteristic scale of the porous medium (the pore diameter) is largely smaller than that of the TPS body, hence the dynamics of oxidant transport at micro-scale is different than the incoming gas regime.

Table 1. Summary of flow tube test conditions: pressure, temperature, oxidation time, mass flow rate, velocity, gas density, gas viscosity and Reynolds number

Sample #	p, kPa	T, K	t, min	$\dot{m}$, mg s^{-1}	u, m s^{-1}	ρ_g, kg m^{-3}	μ_g, mP	Re
a1	1.60	700	60	2.18	0.719	0.00796	0.34288	3.67
a2	1.60	800	60	2.19	0.827	0.00697	0.37563	3.38
a3	1.63	900	60	2.19	0.930	0.00619	0.40688	3.12
a4	1.64	1000	60	2.19	1.034	0.00557	0.43688	2.90
a5	1.63	1100	60	2.21	1.145	0.00507	0.46572	2.74
a6	1.64	1200	60	2.21	1.249	0.00464	0.49355	2.59
a7	1.64	1300	60	2.18	1.335	0.00429	0.52059	2.42
b1	10	700	60	2.19	0.116	0.04977	0.34288	3.70
b2	10	800	60	2.19	0.132	0.04355	0.37563	3.38
b3	10	900	60	2.19	0.149	0.03871	0.40688	3.12
b4	10	1000	60	2.18	0.164	0.03484	0.43688	2.88
b5	10	1100	60	2.19	0.182	0.03167	0.46572	2.72
b6	10	1200	60	2.21	0.200	0.02903	0.49355	2.59
b7	10	1300	60	2.18	0.214	0.02680	0.52059	2.42
c1	60	700	60	2.19	0.019	0.29860	0.34288	3.70
c2	60	800	60	2.19	0.022	0.26128	0.37563	3.38
c3	60	900	60	2.19	0.025	0.23225	0.40688	3.12
c4	60	1000	60	2.19	0.028	0.20902	0.43688	2.90
c5	60	1100	60	2.21	0.031	0.19002	0.46572	2.74
c6	60	1200	60	2.21	0.033	0.17418	0.49355	2.59
c7	60	1300	60	2.21	0.036	0.16079	0.52059	2.45

We applied different techniques to analyze the carbon preform prior to and post flow-tube oxidation. Mass measurements were performed using an analytical balance (AB104S, Mettler-Toledo, LLC, Columbus, OH, United States) with ±0.1 mg accuracy. A caliper was used to document changes in length, inner diameter and outer diameter with ±0.1 mm precision[a]. The bulk density of the material was estimated as the ratio between the mass measured with the balance and the volume calculated from caliper measurements. Initial densities of the specimens were calculated between 175 and 185 kg m^{-3}, with an uncertainty of ±6 kg m^{-3}. Density changes for all the specimens are documented in section III.

In order to determine the exact volume recession due to oxidation for each sample, a suitable post test method was implemented to cope with the brittleness of the carbon preform specimens. The oxidized

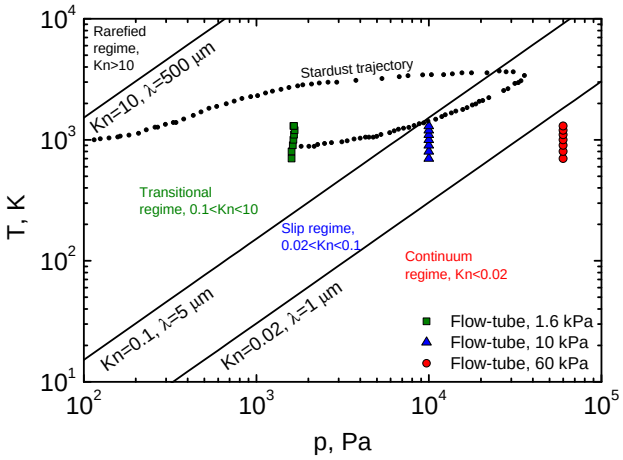

Figure 4. Flow-tube regimes compared to the Stardust trajectory.

[a]The caliper provides 2 digits precision measurements. The quoted uncertainty of ±0.1 mm accounts for errors by its operation from the user.

samples were found to easily crumble into pieces in any attempt of manual extraction from the glass holder. The specimen/holder assembly was impregnated in epoxy resin, by means of an encapsulation chamber (Epovac, Struers A/S, Ballerup, Denmark) capable of 100 mbar terminal vacuum. A resin/hardener mixture (CaldoFix, Struers A/S, Ballerup, Denmark) was poured into a plastic mold hosting the assembly and oven-cured for 2 h at ∼343 K. The encapsulated specimen was then sectioned along axial symmetry plane using a diamond wheel cut-off machine (Accutom-50, Struers A/S, Ballerup, Denmark).

Pictures of the specimen were acquired using a commercial reflex camera, and the area of interest was filtered using Fiji[12] and digitized using Enguage,[13] in order to extract the oxidation profiles coordinates (see Fig. 5). The actual volume loss (recession) was computed by integration the extracted profiles.

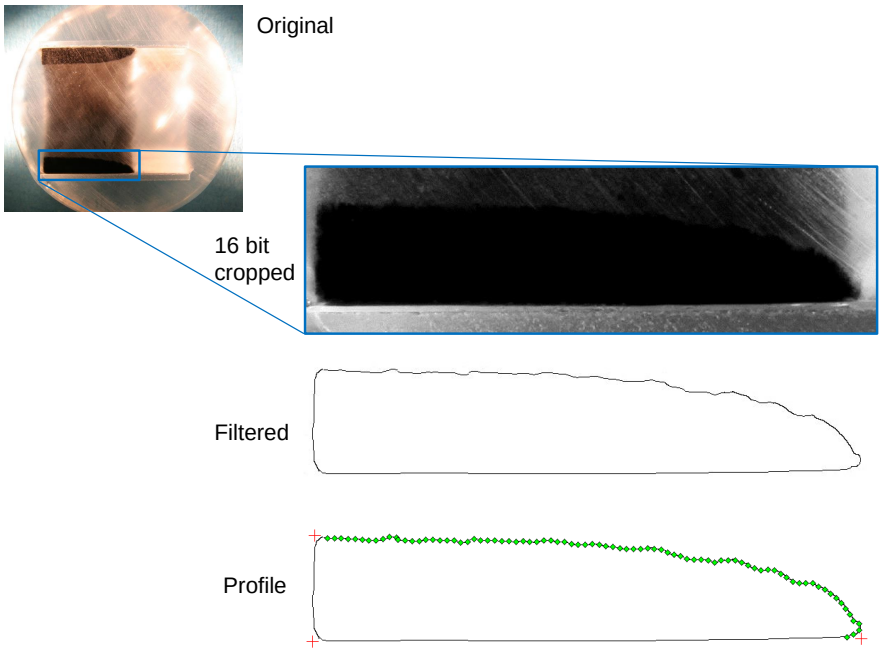

Figure 5. Elaboration of optical microscope images.

An environmental scanning electron microscope (XL30 ESEM, FEI, Hillsboro, OR, United States) was used to characterize the morphology of the fiber prior to and post oxidation tests. Energy dispersive x-ray spectrometry (EDX) allowed analyzing the specimens chemical composition.

III. Results

Micrographs of the virgin material are shown in Fig. 6. During manufacturing, Fiberform's fibers are bonded together with a phenolic resin former, that is fully carbonized through high temperature processing. Carbon bonds between the fibers can be observed at the fibers intersections from the SEM images. Fibers were found to have an average diameter d_f between 9 and 13 µm and an average length l_f between 100 and 500 µm. Bundles or clusters, where multiple fibers are bounded, were observed at several locations throughout the sample. Similar structures were documented for an analogous rayon-based preform material (Calcarb®),[14] used to produce European lightweight ablators as well as PICA-X.

Carbon preform samples, tested in low pressure dry air for 1h, were subjected to ablation by oxidation. The correspondent material loss depends on the temperature to which the specimens were exposed.

Several features could be observed looking at the specimens after the experiments (see Figs. 7, 8 and 9). No macroscopic recession was observed at temperatures below 900 K. Nevertheless, while the material kept its integrity and strength at the lowest temperatures (700 and 800 K), specimens at 900 K were found to be very brittle, a soft touch being sufficient to crumble the material at the front surface (that exposed to the flow). Samples a4 and c3 in Fig. 7 showed the material in early phases of surface recession with top fibers nearly completely eroded by oxygen attack.

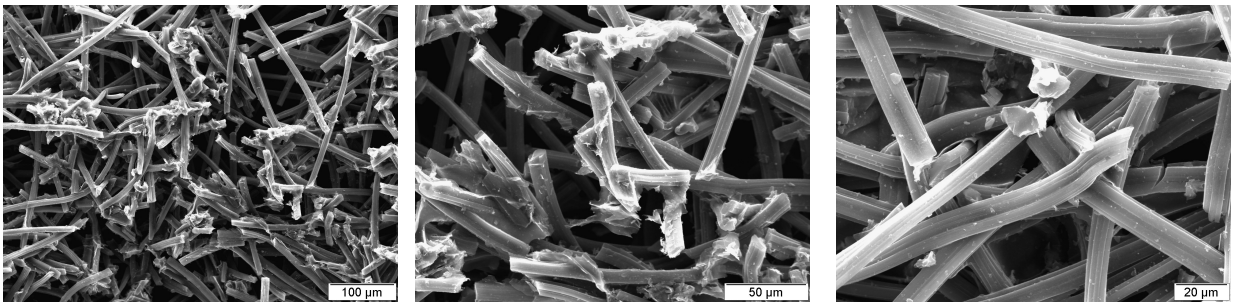

Figure 6. Scanning electron micrographs of virgin carbon preform at different magnification levels.

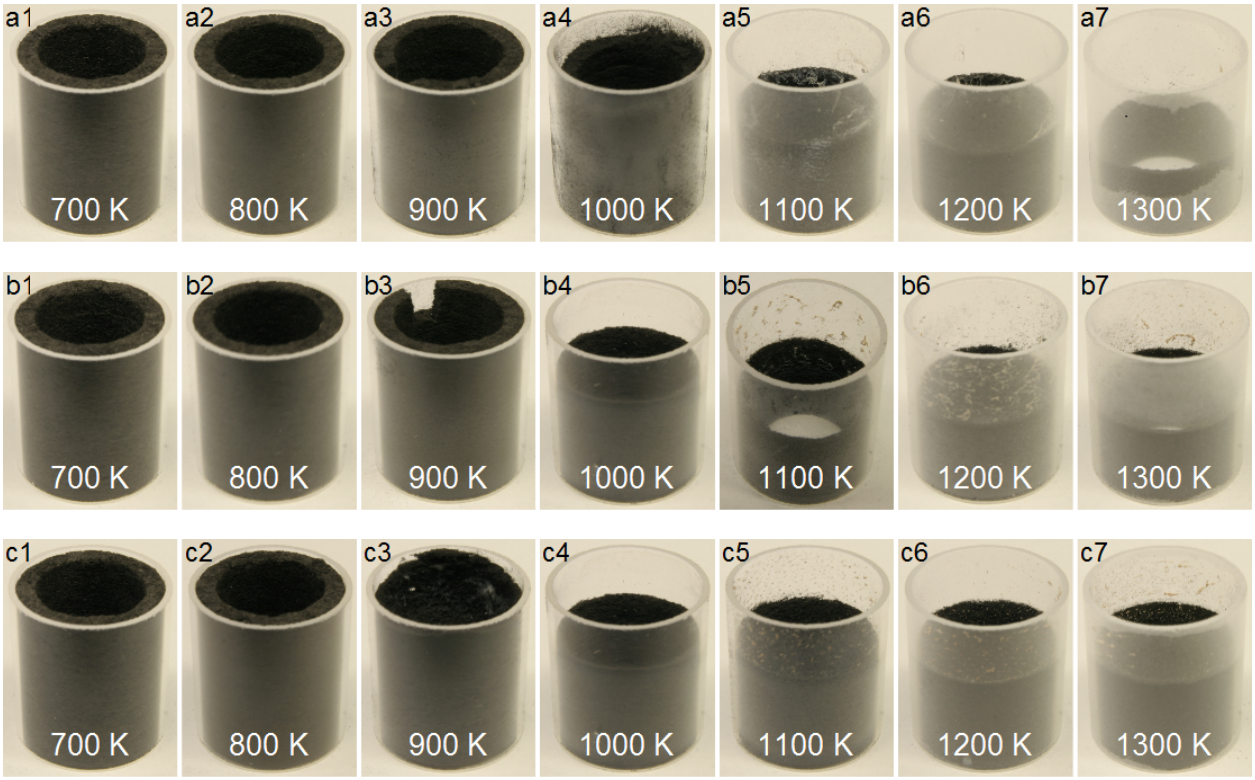

Figure 7. Post test pictures of carbon preform samples in the glass holder. Top row to bottom: specimens tested at 1.6 kPa, 10 and 60 kPa. Small pieces that are missing on the specimens a3 and b3 were extracted for analysis before shooting the present pictures.

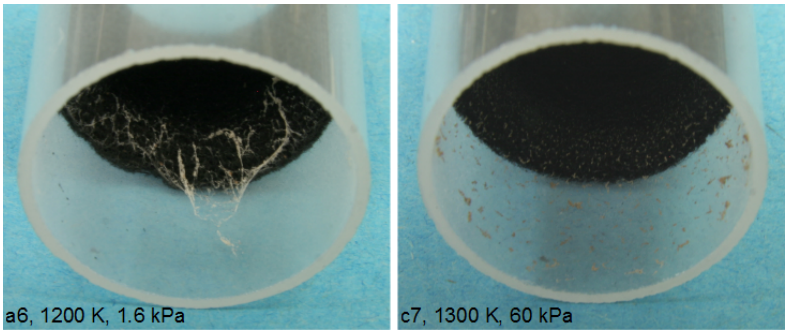

Figure 8. Highlight on impurities depositions over the glass holder walls.

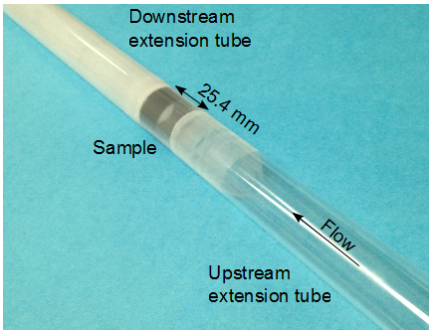

Figure 9. Upstream and downstream extension tubes.

Leftover depositions on the glass walls were observed for specimens tested at 1100 K temperature and above, with different consistency and structure depending on the pressure. Examples are shown in Fig. 8. Depositions at 1.6 kPa presented a whitish color and spider's web-like filamentous structure, easily removable with a gentle blowing action, while specimens at 10 and 60 kPa showed brownish, harder structures, stuck to the glass walls. EDX analyses showed that these are calcium- and oxygen-rich residues, with traces of other species like silicon, sodium, sulfur and potassium. Similar compositions were observed over oxidized carbon fibers at several locations on tested samples, as shown in Fig. 10. Reference 9 reported that the presence of Ca and O traces, found by EDX, suggests oxidation residues to be calcium carbonate ($CaCO_3$). The impurities were believed to act as catalysts for oxidation reactions, providing higher reactivities than those typically reported in the literature.[9,15]

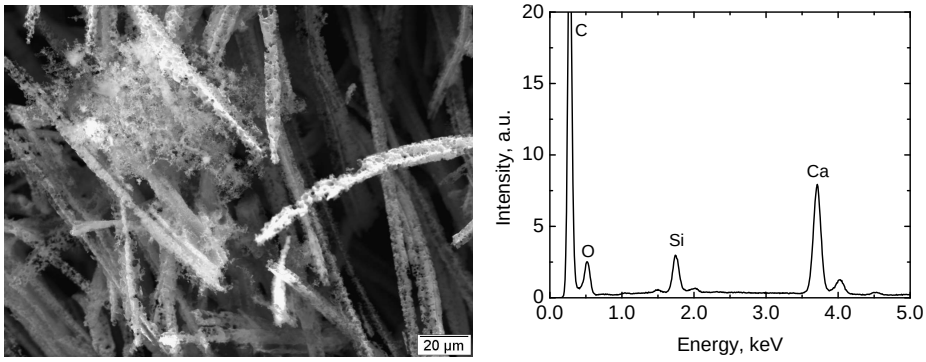

Figure 10. SEM micrograph (left) and EDX analysis (right) of oxidation residues.

Table 2. Mass, volume and density values of carbon preform prior to (subscript 0) and post (subscript f) oxidation

Sample #	p, kPa	T, K	m_0, g	m_f, g	V_0, mm^3	V_f, mm^3	ρ_0, kg m^{-3}	ρ_f, kg m^{-3}
a1	1.60	700	0.781	0.759	4424	4349	176.5	174.6
a2	1.60	800	0.762	0.455	4436	4010	171.8	113.5
a3	1.63	900	0.765	0.448	4479	3629	170.9	123.4
a4	1.64	1000	0.754	0.343	4509	3193	167.3	107.4
a5	1.63	1100	0.749	0.297	4439	2154	168.8	137.7
a6	1.64	1200	0.752	0.267	4500	1852	167.2	144.1
a7	1.64	1300	0.773	0.184	4568	1337	169.1	137.7
b1	10	700	0.749	0.721	4350	4312	172.2	167.2
b2	10	800	0.755	0.502	4556	3972	165.6	126.3
b3	10	900	0.766	0.420	4389	3890	174.5	108.1
b4	10	1000	0.760	0.356	4391	2545	173.1	139.7
b5	10	1100	0.732	0.318	4440	2001	164.8	158.7
b6	10	1200	0.733	0.287	4381	1751	167.3	163.7
b7	10	1300	0.838	0.256	4522	1788	185.4	143.2
c1	60	700	0.756	0.705	4383	4378	172.5	161.1
c2	60	800	0.750	0.450	4323	3969	173.4	113.5
c3	60	900	0.745	0.381	4446	2944	167.7	129.3
c4	60	1000	0.773	0.404	4405	2302	175.5	175.3
c5	60	1100	0.752	0.382	4347	2240	173.0	170.6
c6	60	1200	0.754	0.363	4400	2247	171.4	161.4
c7	60	1300	0.744	0.245	4419	2202	168.3	111.0

Figure 9 shows a post test picture of the extension glass tubes that provide continuity with the sample. One can notice that the downstream portion was completely covered by a whitish opaque scale, likely to be caused by deposition of combustion residues on the walls. Interestingly, the same deposition was observed on the tube preceding the sample, suggesting diffusion of outgassing products up to almost 5 cm upstream the specimen. Attempts were undertaken to clean the tubes with little success. The residues are tenaciously calcified to the glass walls.

Table 2 lists changes in mass, volume and density of carbon preform samples measured prior to and post flow-tube testing. The volume of the virgin material was calculated from caliper measurements of inner diameter, outer diameter and length assuming an ideal (hollow) cylindrical shape. Post test value were calculated integrating the digitized profiles extracted from encapsulated samples, shown in Fig. 11. The profiles illustrate the actual shape of the samples after one hour of oxidation at the specified conditions.

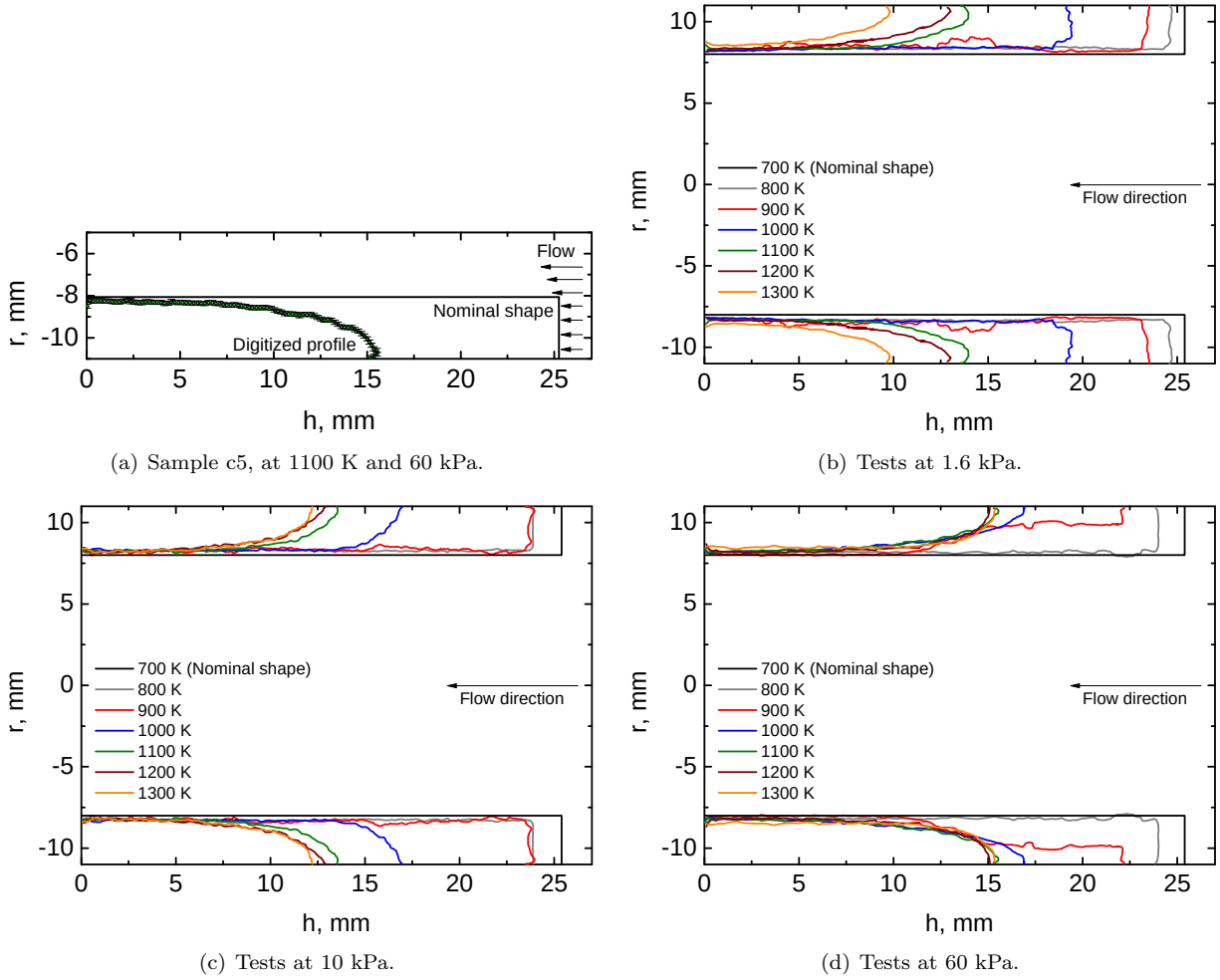

(a) Sample c5, at 1100 K and 60 kPa.

(b) Tests at 1.6 kPa.

(c) Tests at 10 kPa.

(d) Tests at 60 kPa.

Figure 11. Digitized oxidized surface profiles of ablated carbon preform samples. Plot (a) shows the profile on Fig. 5 with the associated error bars, documenting the degree of accuracy that can be obtained with the present procedure.

Percent mass loss and recession are plotted in Fig. 12. As expected, the general trend of an increasing mass loss with increasing temperature was observed. The $\Delta m/m$ rate slows at temperatures higher that 900 K, reaching a plateau around 1200 K, and increases again beyond 1300 K. This behavior is most pronounced at the highest pressure level. For temperatures higher than 900 K, a slight increase in mass loss with decreasing pressure can be noticed. Further experiments and more refined data shall be carried out to consolidate these observations.

The onset of oxidation and subsequent trend of mass loss, presented in Fig. 12, are similar to that of B'_c ablation curves for carbon in air[16] and are commonly documented in the literature on carbon materials

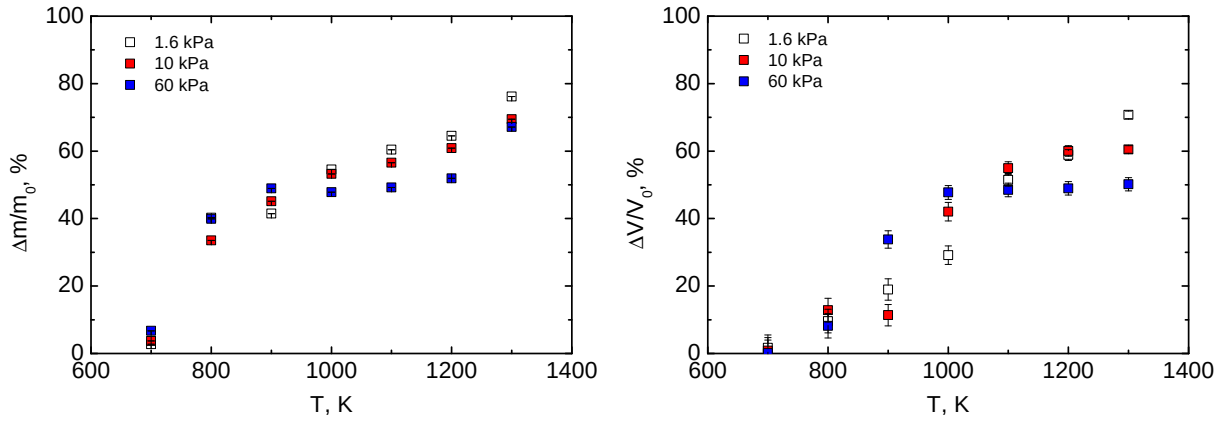

Figure 12. Mass (left) and volume (right) loss as a function of surface temperature.

oxidation at high temperature. This is, of course, not unexpected as the B'_c curves are derived under chemical equilibrium assumptions, and it is most likely the case with the present experiment. It has to be remarked that B'_c curves are derived without accounting for the porosity of the material, while the experiments are naturally accounting for it into the oxidation process. One explanation is that, even though it is a volumetric phenomenon, most of the erosion of C might occur near the surface. The configuration of the sample, where the hot gas is allow to freely go through the sample without being necessarily forced into the porous material, would also amplify this behavior.

Although, as mentioned, no macroscopic recession was observed for specimens tested at temperature from 700 to 900 K by measuring their length, a non-negligible volume loss could be calculated by integrating the oxidized surface profiles. To further assess this, it is worth to analyze the competition between oxidation reactions and diffusional transport at the flow-tube conditions. A dimensionless parameter that is used to characterize such effects for porous materials is the Thiele number:

$$\Phi = \frac{L}{(\mathcal{D}_{\text{eff}}/s_f k_f)^{1/2}} \tag{1}$$

where L is a characteristic length of the model, $\mathcal{D}_{\text{eff}}$ is the effective diffusion coefficient, s_f is the specific surface of the porous medium and k_f is the fiber reactivity. At high Thiele numbers, ablation is mostly a surface phenomenon, since it is limited by a slow diffusional transport. Conversely, when diffusion is high enough to feed a large flux of reactants for chemical reactions and the reactivity is relatively slow, then the depths of the ablation zone becomes larger (typically larger than the fiber scale) and volumetric ablation is promoted.

Here we use the sample wall thickness w as reference length ($L = w = 3$ mm).

The effective diffusion coefficient $\mathcal{D}_{\text{eff}}$ for an isotropic porous medium, is given by $\mathcal{D}_{\text{eff}} = \varepsilon\mathcal{D}_{\text{ref}}/\eta$ where ε is the porosity, η the tortuosity and $\mathcal{D}_{\text{ref}}$ the reference diffusivity. The porosity of Fiberform is estimated to be 0.9 by means of micro-tomography measurements.[17] To calculate the reference diffusivity, one should account for the orthotropy of the material: during the manufacturing process of Fiberform, the fibers tend to align parallel to the direction of the pressing plane,[18] yielding different $\mathcal{D}_{\text{ref}}$ in the planar and transverse direction. A rigorous method consists of computing x-y and z directional diffusivities using random-walk direct numerical simulations.[6] Here, since we are only interested to an order of magnitude estimation of Φ, we neglect these differences and we use Bosanquet's relation to express the reference diffusivity as:

$$\mathcal{D}_{\text{ref}}^{-1} = \mathcal{D}_b^{-1} + \mathcal{D}_K^{-1} = (1/3\bar{v}\bar{\lambda})^{-1} + (1/3\bar{v}d_p)^{-1} \tag{2}$$

where $\mathcal{D}_b$ and $\mathcal{D}_K$ are the bulk and Knudsen diffusivity respectively. The mean free path (in meters) is calculated as[19] $\bar{\lambda} = 9.5 \times 10^{-8} \cdot 10^5 T \cdot (298p)^{-1}$, the mean pore diameter for Fiberform is 50 µm[6] and the mean molecular velocity is estimated by kinetic theory as $\bar{v} = (8k_B T/(\pi m))^{1/2}$. The tortuosity η depends on the Knudsen number and on the orientation as well. Data can be found in Ref. 6, calculated for a random

fibrous medium. For the present calculations of $\mathcal{D}_{\text{ref}}$ we use an average value between x-y and z directions tortuosities.

The specific surface area s_f, in the approximation of the fibers as cylinders that reduce in diameter from $d_{f,0}$ to d_f, can be written as:

$$s_f = 4\varepsilon_{f,0}\frac{d_f}{d_{f,0}^2} \tag{3}$$

where $\varepsilon_{f,0}$ is the initial fiber volume fraction. Average measurements from the scanning electron micrographs of virgin and oxidized carbon fibers allows to reasonably assume $d_{f,0}$ ~11 µm and d_f ~5 µm.

To complete the calculation of the Thiele number, k_f is needed. The underlying behind the experiment presented in the paper is to provide a set of data to extract the fiber reactivity by calibration of a numerical model to the match the measured oxidation profiles. An effort towards this aim is currently ongoing and will be presented in forthcoming publications. A common approach proposed in the literature for reactivity coefficients is to use an Arrhenius formulation with activation energy E_a, that reads:

$$k_f = Ae^{-E_a/(RT)} \tag{4}$$

For the present estimation of Φ we use E_a ~120 kJ mol^{-1} and a pre-exponential factor A=100 m s^{-1}, as given in Ref. 6, based on previous investigation con carbon fiber-based materials.[15,20,21,22] The proposed activation energy is also in agreement with data from Rosner and Allendorf on isotropic graphite.[23,24] It is acknowledged here that, any assumption on k_f values is easily questionable. Indeed discrepancies up to several order of magnitude can be found among literature data, the reasons being multiple, examples being different manufacturing processes and thermal treatments of the materials, different experimental conditions as atmospherics gases, reactants, pressures, diffusion effects and so forth. Therefore, dedicated measurements should be carried out on the very material of interest at meaningful test conditions for its application, any time k_f is needed.

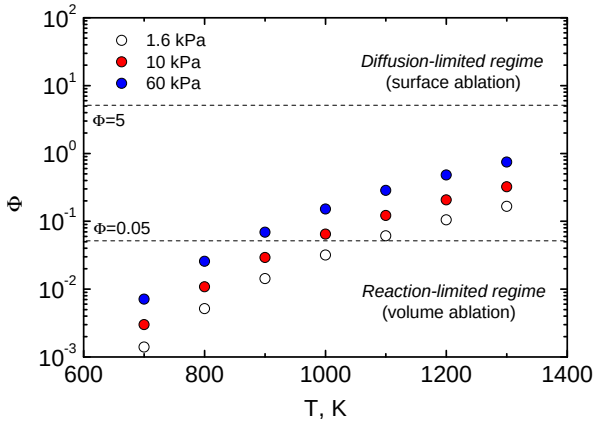

Figure 13. Estimated porous medium regime for the flow-tube test conditions.

Thiele numbers for the flow-tube test conditions, shown in Fig. 13, suggest that for experiments at the lowest temperature and pressure a reaction-limited regime prevails. This is in agreement with what is observed in $\Delta m/m$ and $\Delta V/V$ plots, where, at such condition, mass is lost with minor volume change: diffusion is high enough with respect to reaction to provide in-depth oxidation and limited recession. As pressure and temperature increase, the depth of the oxidation decreases and surface and volume recession tend to equilibrate.

In addition to diffusional effects into the porous medium, it is also worthwhile to consider the diffusion/reaction competition at the flow/surface interface. This is described by the Damköhler number:

$$\text{Da} = \frac{\delta_r k_{s,\text{eff}}}{\mathcal{D}} \tag{5}$$

Da compares a surface effective reaction rate $k_{s,\text{eff}}$ to the rate of reactants diffusion to the wall $\mathcal{D}/\delta_r$, being δ_r the thickness of the reacting boundary layer. Da is small (<0.01) in reaction-limited regime and high (>100) in diffusion-limited regime.

We use the maximum possible size of the boundary layer for δ_r (that is half of the tube diameter, $\delta_r = D/2 = 8$ mm). Numerical simulations of the flow inside the tube will allow to refine this conservative assumption in the future, yet without altering our conclusions.

For a multi-component mixture, it is possible to compute the average species diffusion coefficients for the species i, according to Fick's law, as:

$$\mathcal{D}_i = \frac{1 - x_i}{\sum_{j \neq i} \frac{x_j}{\mathscr{D}_{i,j}}} \tag{6}$$

The binary diffusion coefficients $\mathscr{D}_{i,j}$ are given by:

$$\mathscr{D}_{i,j} = \frac{3}{16} \left(\frac{2\pi k_B T \left(m_i + m_j\right)}{m_i m_j} \right)^{1/2} \frac{1}{n \bar{Q}_{i,j}^{(1,1)}} \tag{7}$$

being m_i and m_j the atomic (or molecular) mass of the diffusing species i and j and $n = p/(k_B T)$ the number density. The diffusion cross-sections $\bar{Q}_{i,j}^{(1,1)}$ can be obtained from fitting expressions provided by Capitelli et al.[25] Calculations of O_2 mole fraction x_{O_2} for a themo-chemical equilibrium mixture at present the experimental conditions and effective reactivities of $k_{s,\text{eff}} \approx \mathcal{O}(10^{-2})$,[15] provide Damköhler numbers below 10^{-2}, 10^{-1} and 10^{0} at 1.6, 10 and 60 kPa respectively, confirming that the diffusion limitation is prevented at all flow conditions in the reactor.

The fiber-scale oxidation of the specimens can be described by the micrographs shown in Fig. 6. These pictures clearly show that mass is lost at localized "active" sites where oxygen molecules react with carbon, resulting in pitting patterns distributed over the fiber surface (see Figs. 14(d) to 14(l)). The complete ablation of a single fiber is caused by an increase of the holes spatial density over the surface (rather then an increase of the holes' size), until the whole fiber's surface is covered.

Interestingly, it can be noticed that despite the randomness of the pitting, the distribution of active oxidation locations is uniform throughout the fiber surface, that is there is no higher density of holes at a specific region along the fiber length (like for instance on the upstream portion of a fiber whose aspect ration is oriented in the direction of diffusion of the flow through the pores). As a result fibers show uniform thinning (i.e. diameter reduction) over the whole fiber length. This is true at all temperatures below 1300 K and at the three pressures applied during testing. SEM of specimens tested at the highest temperature showed instead icicle shaped fibers, where the fiber diameter reduces from the bottom to the top of the fiber.

IV. Conclusion

Data were presented from flow-reactor experiments on carbon fiber preform. Twenty-one hollow cylinder models were tested in the NASA Ames flow-tube reactor facility under laminar dry air, at temperatures from 700 to 1300 K and pressures of 1.6, 10 and 60 kPa. Mass loss and recession data were measured and the change of the material morphology at fiber-scale was characterized using scanning electron microscopy. It was found that the microscopic oxidation of fibers occurs at specific sites where oxygen attacks the carbon, forming a pitting pattern distributed over the surface. The oxidation of the fibers leads to a progressive reduction of their diameter. Both visual observation and microscopic analysis showed the presence of combustion residues in between carbon fibers, that EDX analyses confirmed to be calcium- and oxygen-rich structures.

An order of magnitude estimation of Thiele and Damköhler allowed us to assess the diffusion/reaction processes in the porous medium and at the fluid/surface interface. Low pressures ($\leq$ 10 kPa) and low temperatures ($\leq$ 900 K) promote a reaction limited regime in the porous medium, where oxidation is mostly a volumetric process. Thiele number increases as pressure and temperature increase. Most of the experiment are in a transition regime where reaction and diffusion control conditions are balanced. The transport of oxidant to the surface is high enough to prevent any diffusion limitation at the material surface.

A current effort is being undertaken to model the flow-tube environment and the recession of carbon preform by oxidation. This will allow to extract the fiber reactivity for the material of interest and to improve the calculation of Φ and Da. Further work will focus on the study of different geometrical models and different atmospheric gases and conditions, as well as on refining the data at the condition presented in this work. Micro-tomography measurements are also being pursued to improve the characterization of the three-dimensional structure of Fiberform at fiber scale and to provide more accurate data on tortuosities, porosity and other properties. Preliminary results presented in a companion paper at this conference are very encouraging in this respect.[17]

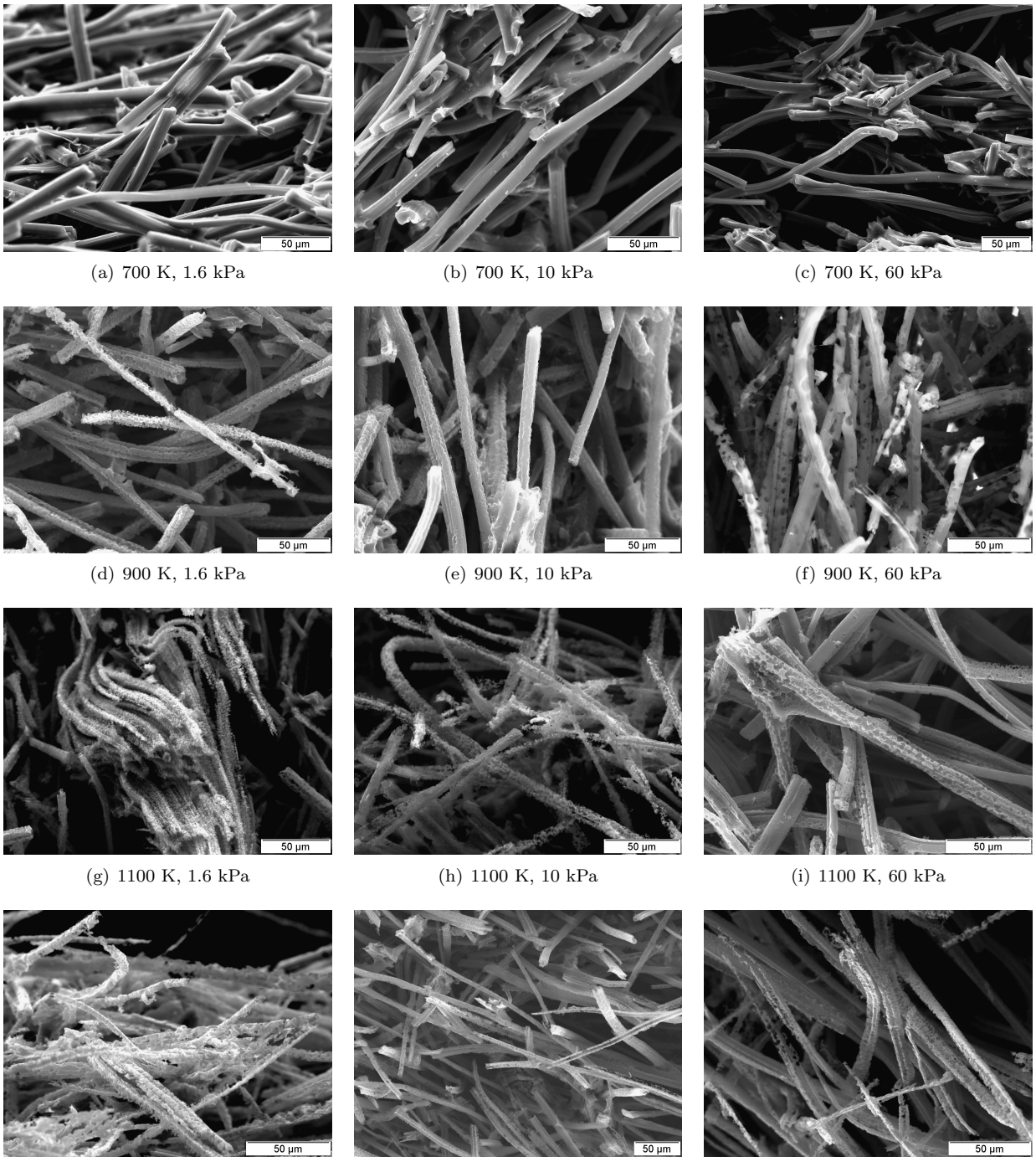

(a) 700 K, 1.6 kPa (b) 700 K, 10 kPa (c) 700 K, 60 kPa

(d) 900 K, 1.6 kPa (e) 900 K, 10 kPa (f) 900 K, 60 kPa

(g) 1100 K, 1.6 kPa (h) 1100 K, 10 kPa (i) 1100 K, 60 kPa

(j) 1300 K, 1.6 kPa (k) 1300 K, 10 kPa (l) 1300 K, 60 kPa

Figure 14. Micrographs of oxidized carbon preform at different flow-tube conditions.

V. Acknowledgements

Financial support to F.P. for this work was provided by NASA SBIR Phase-2 Award NNX10CC53P, and NASA Kentucky EPSCoR Award NNX10AV39A. Support by the Hypersonic EDL program for the effort is gratefully acknowledged. We thank the unwavering encouragements by M.J. Wright (NASA Ames Research Center) and A.M. Calomino (NASA Langley Research Center). We are also thankful to J. Chavez Garcia (ERC, Inc.) for the support on scanning electron microscopy, J.W. Ridge (ERC, Inc.) for the assistance at the flow-tube laboratory and M. Gusman (ERC, Inc.) for the training on samples' encapsulation. The review comments by F.S. Milos (NASA Ames Research Center) and Y.-K. Chen (NASA Ames Research Center) are greatly appreciated.

References

[1]Chen, Y.-K. and Milos, F. S., "Ablation and Thermal Response Program for Spacecraft Heatshield Analysis," *Journal of Spacecraft and Rockets*, Vol. 36, No. 3, 1999, pp. 475–483.

[2]Chen, Y.-K. and Milos, F. S., "Two-Dimensional Implicit Thermal Response and Ablation Program for Charring Materials," *Journal of Spacecraft and Rockets*, Vol. 38, No. 4, 2001, pp. 473–481.

[3]Chen, Y.-K. and Milos, F. S., "Ablation, Thermal Response, and Chemistry Program for Analysis of Thermal Protection Systems," *Journal of Spacecraft and Rockets*, Vol. 50, No. 1, Jan. 2013, pp. 137–149.

[4]Bose, D., White, T., Santos, J., Feldman, J., Mahzari, M., Olson, M., and Laub, B., "Initial Assessment of Mars Science Laboratory Heatshield Instrumentation and Flight Data," *51th AIAA Aerospace Sciences Meeting including the New Horizons Forum and Aerospace Exposition*, AIAA 2013-0908, Grapevine, TX, 2013.

[5]Mahzari, M., White, T., Braun, R., and Bose, D., "Preliminary Analysis of the Mars Science Laboratory's Entry Aerothermodynamic Environment and Thermal Protection System Performance," *51th AIAA Aerospace Sciences Meeting including the New Horizons Forum and Aerospace Exposition*, AIAA 2013-0185, Grapevine, TX, 2013.

[6]Lachaud, J., Cozmuta, I., and Mansour, N. N., "Multiscale Approach to Ablation Modeling of Phenolic Impregnated Carbon Ablators," *Journal of Spacecraft and Rockets*, Vol. 47, No. 6, 2010, pp. 910–921.

[7]Ellingham, H. J. T., "Reducibility of Oxides and Sulfides in Metallurgical Processes," *Journal of the Society of Chemical Industry*, Vol. 63, No. 5, 1944, pp. 125.

[8]Chase, Jr., M. W., "NIST-JANAF Thermochemical Tables (Part I and II)," *Journal of Physical and Chemical Reference Data Monographs*, No. 9 in Monograph, American Institute of Physics, 1998.

[9]Lachaud, J., Mansour, N. N., Ceballos, A., Pejaković, D., L., Z., and Marschall, J., "Validation of a Volume-Averaged Fiber-Scale Model for the Oxidation of a Carbon-Fiber Preform," *42th AIAA Thermophysics Conference*, AIAA 2011-3640, Honolulu, HI, USA, 2011.

[10]McBride, B. J. and Gordon, S., "Computer Program for Calculation of Complex Chemical Equilibrium Compositions and Applications," Reference Publication 1311, NASA, 1996.

[11]Trumble, K. A., Cozmuta, I., Sepka, A. S., Jenniskens, P., and Winter, M., "Postflight Aerothermal Analysis of the Stardust Sample Return Capsule," *Journal of Spacecraft and Rockets*, Vol. 47, No. 5, 2010, pp. 765–774.

[12]Schindelin, J., Arganda-Carreras, I., Frise, E., Kaynig, V., Longair, M., Pietzsch, T., Preibisch, S., Rueden, C., Saalfeld, S., Schmid, B., Tinevez, J.-Y., White, D. J., Hartenstein, V., Eliceiri, K., Tomancak, P., and Cardona, A., "Fiji: an Open-Source Platform for Biological-Image Analysis," *Nature Methods*, Vol. 9, No. 7, 2012, pp. 676–682.

[13]Mitchell, M., "Engauge Digitizer - Digitizing software," http://digitizer.sourceforge.net/.

[14]Helber, B., Chazot, O., Magin, T., and Hubin, A., "Ablation of Carbon Preform in the VKI Plasmatron," *43rd AIAA Thermophysics Conference*, AIAA 2012-2876, New Orleans, LA, USA, 2012.

[15]Lachaud, J., Bertrand, N., Vignoles, G., Bourget, G., Rebillat, F., and Weisbecker, P., "A Theoretical/Experimental Approach to the Intrinsic Oxidation Reactivities of C/C Composites and of their Components," *Carbon*, Vol. 45, 2007, pp. 2768–2776.

[16]Milos, F. S. and Chen, Y.-K., "Ablation Predictions for Carbonaceous Materials Using Two Databases for Species Thermodynamics," *Journal of Spacecraft and Rockets*, Vol. 50, No. 2, 2013, pp. 245–255.

[17]Mansour, N., Panerai, F., Martin, A., Parkinson, D., MacDowell, A., Fast, T., and Lachaud, J., "Fiber-Scale Ablation Behavior of the Carbon Preform of PICA: Micro-Tomography Measurements, Modeling, and Statical Analysis," *44th AIAA Thermophysics Conference*, AIAA 2013-XXXX, San Diego, CA, USA, 2013.

[18]Marschall, J. and Milos, F. S., "Gas Permeability of Rigid Fibrous Refractory Insulations," *Journal of Thermophysics and Heat Transfer*, Vol. 12, No. 4, 1998, pp. 528–535.

[19]Reid, R. C., Prausnitz, J. M., and Poling, B. E., *The Properties of Gases and Liquids, 4th ed.*, McGraw-Hill, New York, 1987.

[20]Chen, Y.-K. and Milos, F. S., "NavierStokes Solutions with Finite Rate Ablation for Planetary Mission Earth Reentries," *Journal of Spacecraft and Rockets*, Vol. 42, No. 6, 2005, pp. 961–970.

[21]Park, C., *Nonequilibrium Hypersonic Aerothermodynamics*, John Wiley & Sons, New York, 1990.

[22]Lavigne, O., Dorvaux, J., Drawin, S., and Bacos, M., "Oxidation Model for Carbon-Carbon Composites," *4th International Aerospace Planes Conference, Orlando*, AIAA 1992-210, Orlando, FL, 1992.

[23]Rosner, D. E. and Allendorf, H. D., "High Temperature Oxidation of Carbon by Atomic Oxygen," *Carbon*, Vol. 6, No. 4, 1965, pp. 153–156.

[24]Rosner, D. E. and Allendorf, H. D., "Comparative Studies of the Attack of Pyrolytic and Isotropic Graphite by Atomic and Molecular Oxygen at High Temperatures," *AIAA Journal*, Vol. 6, No. 4, 1968, pp. 650–654.

[25]Capitelli, M., Gorse, C., Longo, S., and Giordano, D., "Collision Integrals of High-Temperature Air Species ," *Journal of Thermophysics and Heat Transfer*, Vol. 14, No. 2, 2000, pp. 259–268.